Cell Migration and Cell-Cell Interaction in the Presence of Mechano-Chemo-Thermotaxis

S.J. Mousavi[*], **M.H. Doweidar**[*,†] **and M. Doblaré**[*]

Abstract: Although there are several computational models that explain the trajectory that cells take during migration, till now little attention has been paid to the integration of the cell migration in a multi-signaling system. With that aim, a generalized model of cell migration and cell-cell interaction under multisignal environments is presented herein. In this work we investigate the spatio-temporal cell-cell interaction problem induced by mechano-chemo-thermotactic cues. It is assumed that formation of a new focal adhesion generates traction forces proportional to the stresses transmitted by the cell to the extracellular matrix. The cell velocity and polarization direction are calculated based on the equilibrium of the effective forces associated to cell motility. It is also assumed that, in addition to mechanotaxis signals, chemotactic and thermotactic cues control the direction of the resultant traction force. This model enables predicting the trajectory of migrating cells as well as the spatial and temporal distributions of the net traction force and cell velocity. Results indicate that the tendency of the cells is firstly to reach each other and then migrate towards an imaginary equilibrium plane located near the source of the signal. The position of this plane is sensitive to the gradient slope and the corresponding efficient factors. The cells come into contact and separate several times during migration. Adding other cues to the substrate (such as chemotaxis and/or thermotaxis) delays that primary contact. Moreover, in all states, the average local velocity and the net traction force of the cells decrease while the cells approach the cues source. Our findings are qualitatively consistent with experimental observations reported in the related literature.

Keywords: cell migration, cell-cell interaction, mechanotaxis, chemotaxis, thermotaxis, numerical simulation, finite element method

---

[*] Group of Structural Mechanics and Materials Modelling (GEMM), Aragón Institute of Engineering Research (I3A), University of Zaragoza, Spain. Centro de Investigación Biomédica en Red en Bioingeniería, Biomateriales y Nanomedicina (CIBER-BBN), Spain.

[†] E-mail: mohamed@unizar.es

1   Introduction

Cell migration is a fundamental phenomenon in many physiological and pathological processes including tissue development and repair, morphogenesis, wound healing, immune response as well as cancer metastasis [1, 2 3, 4, 5]. A living cell can be stimulated by many types of cues such as mechanotaxis (durotaxis and tensotaxis) [6, 7, 8], chemotaxis [9, 10, 11] and thermotaxis [12, 13] among others. Each of these cues can activate the cell pseudopodia and lamellipodia to steer the cell towards the most effective or permanent signal [9, 14].

Experiments demonstrate that the cell can recognize stiffer regions in the extracellular matrix (ECM) [15, 16, 17]. For instance, fibroblast cells preferentially move towards stiffer substrates [18, 19, 20]. This phenomenon is known as mechanotaxis which refers to the movement of cells induced by mechanical cues. During this process, the cell senses the stiffness of the substrate by exerting a sensing force which is in general smaller than the externally acting traction force (mechano-sensing process). The traction forces generated by the cell are the resultant of the combined effort of the actin bundles, the actomyosin contractile machinery and the passive mechanical apparatus of the cytoskeleton that, in the end, change the cell shape and propel it [16, 17, 20, 21].

Chemotaxis is another key signal that regulates the direction of cell migration. Different experiments [9, 10, 22, 23] acknowledge that cells reorientate their migration direction when they are subjected to a chemoattractant or chemorepellant agent. For instance, exposing a cell to a cyclic Andenosine Monophosphate (cAMP) gradient activates cAMP receptors and their associated G-proteins which cause cell reorientation [24]. However the comprehensive reason for this phenomenon is still unknown. Some authors however, attribute this effect to a "compass" that the cell may have [22, 23]. The possible features of that compass vary, but a hypothesis is the existence of a simple "compass needle" inside the cell formed by a localized signal in the direction of the chemotaxis. In contrast, some researchers reject this theory and address that this internal compass does not exist but the cell orients itself simply by its pseudopods [11]. Till now, there are few computational models that consider the cell motility associated to chemotaxis. For instance, Neilson et al. [25] modeled cell movement in absence and in presence of a chemoattractant by means of the Level Set Method. The weakest point of their model is that they ignored the effect of the mechanical properties of the substrate. Moreover, in the absence of chemotaxis, they considered a totally random cell movement which is not accurate enough.

Cell thermotaxis has been known for many years in trophoblast cells [13]. In vivo, thermotaxis is complementary to chemotaxis. For example, in the oviduct (a long

region of female genitals) cells are guided by thermotaxis while in fertilization sites (a shorter area) they are steered by means of chemotaxis [26]. Moreover, trophoblast cells move towards the inner membrane of the uterus (warmer region) due to thermotaxis [26]. Extravillous trophoblasts also migrate from the tips of the anchoring villi that surround the developing blastocyst to the distal portions of the uterine spiral arteries through the maternal deciduae [27]. Thermotaxis is also the reason for motility of individual amoebae of dictyostelium discoideum on a thermal gradient. These amoebae show positive thermotaxis at temperatures between 14°C and 28°C shortly (3 hr) after food depletion [28]. Experiments by Higazi et al. [13] demonstrated that cultured human trophoblasts are influenced by thermal gradient. They reported that human trophoblastic cells sense differences of less than 1°C above or below physiological temperature.

The present work is an extension of a previous mechanotactic model [20]. This new approach is capable of predicting cell migration through a 3D substrate under the influence of all these effective signals simultaneously. In this model it is assumed that boundaries of the cells (cells membrane) are connected to cell centroid via elastic-linear springs. This provides a straightforward formulation which enables us to develop a 3D finite element model based on the equilibrium of traction forces acting on cell motility. Several numerical experiments are presented to demonstrate the predictive capability of the model for two interacting cells in a substrate with gradient stiffness. The obtained results are qualitatively validated by means of available experimental results [15, 9, 13]. Some of our findings match with these experimental studies while others provide new insights for new and future experimental set-ups.

2 Constitutive model

In this section, the biological processes occurring in the cell are linked with the formation and dissociation of the stress fibers, as well as the associated generation of tension and contractility. The relevant role of each cell component is discussed and the effective forces acting on the cell body are calculated. From that, the velocity and polarization direction of the cell are computed based on equilibrium of calculated effective forces.

2.1 *Net cell stress transmitted by a single cell to the ECM*

The cellular elements with a relevant function on the cell motility mechanism can be divided in two main parts, active and passive. The former are due to the change in the overlapping between myosin and actin elements of the cytoskeleton (CSK), while the latter are related to the action of the CSK microtubules and the cell membrane. In a very simplified way, the constitutive behavior of each element of the

cell can be approximated by a linear-elastic spring. Therefore, the effective stress transmitted by the cell to the ECM can be calculated by [19, 20]

$$\sigma_{cell} = \begin{cases} K_{pas}\varepsilon_{cell} & \varepsilon_{cell} < \varepsilon_{\min} \; or \, \varepsilon_{cell} > \varepsilon_{\max} \\ \frac{K_{act}\sigma_{\max}(\varepsilon_{\min}-\varepsilon_{cell})}{K_{act}\varepsilon_{\min}-\sigma_{\max}} + K_{pas}\varepsilon_{cell} & \varepsilon_{\min} \leq \varepsilon_{cell} \leq \tilde{\varepsilon} \\ \frac{K_{act}\sigma_{\max}(\varepsilon_{\max}-\tilde{\varepsilon})}{K_{act}\varepsilon_{\max}-\sigma_{\max}} + K_{pas}\varepsilon_{cell} & \tilde{\varepsilon} \leq \varepsilon_{cell} \leq \varepsilon_{\max} \end{cases} \qquad (1)$$

where K_{pas} and K_{act} stand for the stiffness of passive and active cellular elements respectively, and ε_{cell} and $\sigma_{\max}$ denote the internal strain of the cell and the maximum contractile stress exerted by the actin-myosin machinery respectively. Finally, $\tilde{\varepsilon} = \sigma_{\max}/K_{act}$.

2.2   *Effective forces on translocation of the cell*

We assume that the cell exerts sensing forces at each finite element node of the cell membrane towards its centroid. The cell subjected to these sensing forces gets strained so that the effective cell stress, $\sigma cell$, corresponding to each finite element node can be obtained. Traction forces are generated due to the contraction of the actin-myosin apparatus. These have been considered to be proportional to the effective stress transmitted by the cell to the ECM and to the cell area, S. Therefore, the nodal traction force acting at the ith finite element node of the cell membrane towards the cell centroid can be obtained as [20]

$$\mathbf{F}_i^{trac} = \sigma_{cell}Skn_r\psi\mathbf{e}_i \qquad (2)$$

where k is the binding constant of the integrins, n_r the total number of available receptors, and ψ the concentration of the ligands at the leading edge of the cell. $\mathbf{e}_i$ is a unit vector passing from the ith node towards the cell centroid. Therefore, the net traction force acting on the whole cell body, $\mathbf{F}_{net}^{trac}$, is calculated as:

$$\mathbf{F}_{net}^{trac} = \sum_{i=1}^{n} \mathbf{F}_i^{trac} \qquad (3)$$

where n is the number of the cell nodes associated to the cell membrane.

On the contrary, the drag force comes from the viscous resistance of the ECM to cell motility. We assume a linear viscoelastic ECM and the cell as a sphere moving through a Newtonian infinitely viscose medium [20, 29]. So, the drag force can be expressed as

$$\mathbf{F}_{drag} = 6\pi r\eta v \qquad (4)$$

where r is the cell radius, η stands for the effective viscosity of the matrix, and v denotes the cell velocity.

Moreover, the cell spreads and retracts a kind of force that is generated by local protrusions to probe the substrate cues. It is generated by actin polymerization which is different from the cytoskeletal contractile force transmitted to the ECM [29]. This force is here implemented by a protrusion force which is a considered random in both direction and magnitude. It is of the same order of the traction force but normally lower [30, 20, 31]. Here, it is randomly estimated in function of the net traction force as

$$\mathbf{F}_{prot} = k\mathbf{F}_{net}^{trac}\mathbf{e}_{rand} \tag{5}$$

where $\mathbf{e}_{rand}$ is a random unit vector and k is a random number, $0 \leq k < 1$ [20]. It is reported that the presence of chemotaxis and thermotaxis regulate independently the cell migration [32, 5]. As the cell exerts traction forces to move its body through the substrate, the mechanotactic cues always exist despite the presence or absence of other cues. In contrast, chemo and thermotaxis cues only affect the cell polarization direction by modulating the direction of the pseudopods. Therefore, by this regulation of the cell polarization direction, the cell reorients, on average, along the gradient of these signals.

Consequently, the force equilibrium on cell locomotion yields

$$\mathbf{F}_{drag} + \mathbf{F}_{eff} + \mathbf{F}_{prot} = \mathbf{0} \tag{6}$$

where $\mathbf{F}_{eff}$ is the effective force due to mechanotaxis, chemotaxis and thermotaxis whose magnitude and direction depend on the net traction force and the direction of each cue respectively. They will be derived in detail in the next section.

2.3 Migration direction and velocity

In the sensing process the cell is subjected to sensing forces that, in the model here proposed, act at each finite element node of the cell membrane towards its centroid (Fig. 1b). The deformed cell subjected to those sensing forces is represented by dashed lines in Fig. 1c. Therefore, the cell internal strain can be written as

$$\varepsilon_{cell} = \frac{AB}{OA} \tag{7}$$

Once the internal strain of the cell is calculated, using Eqs. (1) and (3), σ_{cell} and the net traction force can be obtained.

It is important to note that the internal deformation created by the sensing forces at each node of the cell membrane is negative (cell exerts contraction forces toward its centroid and always compresses the cell). Therefore, nodes with lower internal deformation will have a higher tension force [20]. As all the traction forces are

acting towards the cell centroid, the resultant of these traction forces will have the direction of minimum internal deformation Eq. (3). Consequently, the opposite direction of the net traction force represents the mechanotaxis reorientation of the cell [20]. The unit vector of the mechanotaxis that reorients the cell, $\mathbf{e}_{mech}$ can then be defined as

$$\mathbf{e}_{mech} = -\frac{\mathbf{F}_{net}^{trac}}{\|\mathbf{F}_{net}^{trac}\|} \tag{8}$$

In the presence of other cues such as chemo and thermotaxis, the reorientation of the cell depends not only on the cell mechanosensing process, but also on these specific signals. Let us assume $\mathbf{e}_{ch}$ and $\mathbf{e}_{th}$ represent unit vectors associated to cell reorientation due to chemical and thermal gradients respectively. Therefore

$$\mathbf{e}_{ch} = \frac{\nabla C}{\|\nabla C\|} \tag{9}$$

$$\mathbf{e}_{th} = \frac{\nabla T}{\|\nabla T\|} \tag{10}$$

where ∇ is the gradient operator and C and T are the chemoattractant concentration and the temperature respectively.

An activation signal in the presence of chemotaxis and/or thermotaxis triggers actin polymerization and myosin phosphorylation. Since the properties of a typical cell as well as the parameters of its ECM will not change in the presence of these cues, it is assumed that the magnitude of the net traction force exerted by the cell is independent of these two cues, while it is a function of cell and substrate characteristics. Therefore, the presence of these signals only changes the effective direction of the previously calculated net traction force. Besides, we consider that the realignment of this force in presence of these cues is proportional to the chemotactic and thermotactic gradients and their associated effective factors respectively. Consequently from (6) and according to Fig. 1c, the effective force,

$\mathbf{F}_{eff}$ in the presence of the chemotaxis and thermotaxis can be defined as

$$\mathbf{F}_{eff} = \mathbf{F}_{net}^{trac}(\mu_{mech}\mathbf{e}_{mech} + \mu_{ch}\mathbf{e}_{ch} + \mu_{th}\mathbf{e}_{th}) \tag{11}$$

where μ_{mech} μ_{ch} and μ_{th} are the efficient factors associated to mechanotaxis, chemotaxis, and thermotaxis cues respectively, such that $\mu_{mech} + \mu_{ch} + \mu_{th} = 1$.

Moreover, the local velocity, υ and net polarization direction, $\mathbf{e}_{pol}$, of the cell can be calculated by

$$\upsilon = \frac{\|\mathbf{F}_{drag}\|}{6\pi r\eta} \tag{12}$$

(a)

(b)

(c)
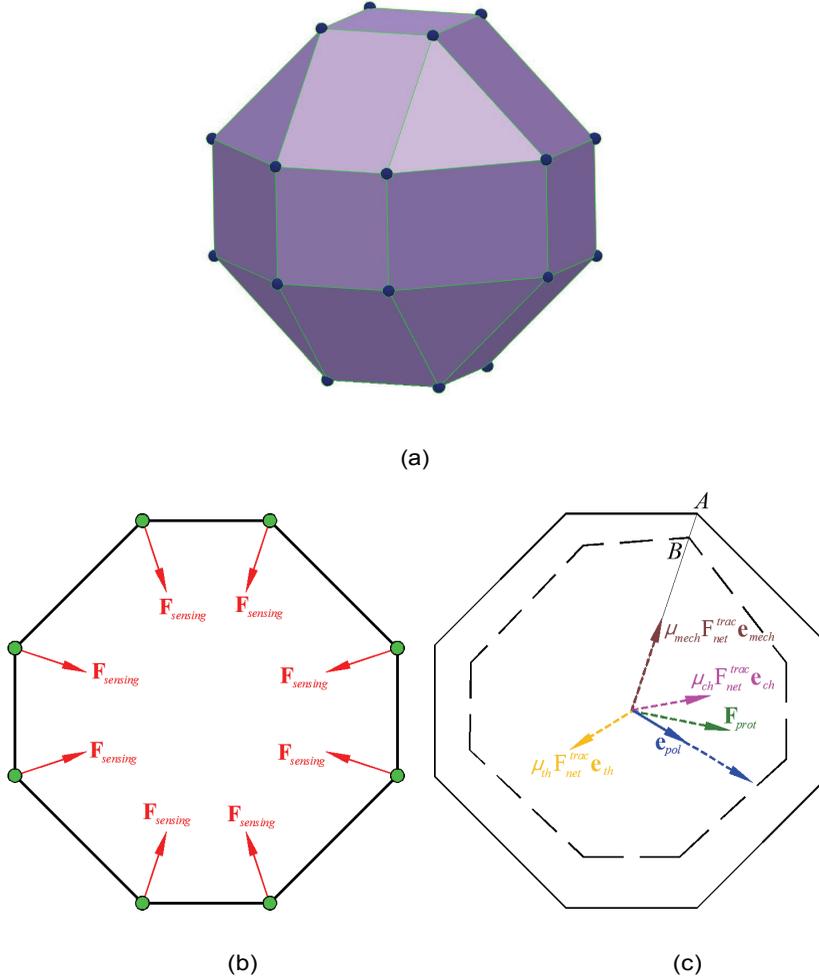
Figure 1: Calculation of the internal deformation and reorientation of a cell. a. Spherical cell shape with finite element discretization. b. Exerted sensing forces at each node of the cell membrane. c. Deformed cell (dashed line) due to mechanosensing in the presence of mechanotaxis, chemotaxis and thermotaxis, with $\mathbf{e}_{mech}$, $\mathbf{e}_{ch}$, and $\mathbf{e}_{th}$ the unit vectors in the direction of each cue respectively and μ_{mech}, μ_{ch}, and μ_{th} their associated efficient factors. $\mathbf{F}_{net}^{trac}$ is the magnitude of the net traction force while $\mathbf{F}_{prot}^{trac}$ is the random protrusion force.

$$\mathbf{e}_{pol} = -\frac{\mathbf{F}_{drag}}{\left\|\mathbf{F}_{drag}\right\|} \tag{13}$$

Using (12) and (13), the displacement vector of an individual cell over the time increment, $\mathbf{d}$ is obtained by

$$\mathbf{d} = \upsilon \tau \mathbf{e}_{pol} \tag{14}$$

2.4 Cell-cell interaction

In the interaction between cells, the same formulae are valid to calculate the acting forces on the cell and define the migration direction of each individual cell. For discretization purposes and to avoid interference of two cells we assume

$$\left\|\mathbf{r}_j - \mathbf{r}_i\right\| \geq 2r \tag{15}$$
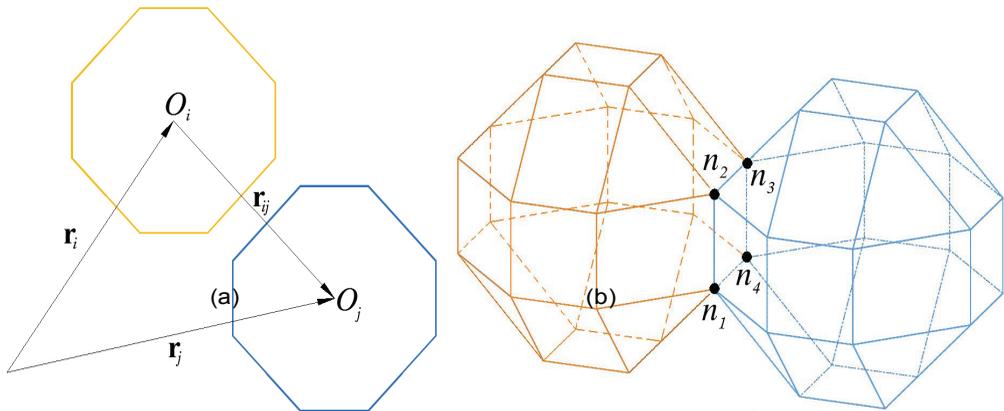
Figure 2: a. Calculation of the position vector of each cell and the distance between the centroids of two cells. The minimal distance between their centroids is equal to the proposed cell diameter. b. Interaction between two cells in contact. Here, for the assumed cell shape and discretization, two cells can have four common nodes as a maximum.

where $\mathbf{r}_i$ and $\mathbf{r}_j$ are the position vectors of each cell centroid (Fig. 2a). Actually, the cells inside a multicellular system do not maintain a spherical shape but deform to become adjacent to each other occupying the entire matrix [20, 33]. Therefore, we have assumed that when two or several cells touch each other (see Fig. 2b), the

common points of the contacting cells are not able to send out any pseudopod to the substrate [20, 34, 35]. As an immediate consequence, for two interacting cells, we assume that the cells do not exert any sensing force at those nodes unless they get separated again. Note that despite there is no sensing force in these nodes, their corresponding nodal traction force is not zero.

3   Numerical and experiments results

The model presented above has been implemented into the commercial FE software ABAQUS [36] using a user subroutine. Fig. 3 presents the algorithm of that routine. Throughout the following simulations, we applied the model to a $400\times200\times200$ μm substrate with linear stiffness gradient which changes from 80 kPa at x=0 to 100 kPa at x= 400 μm. All the substrate surfaces are considered to be free. The substrates are meshed by 16000 regular hexahedral elements with 18081 nodes, while there is no external force acting on the substrate. The user subroutine is run for about 200 steps with one time step approximately equal to 10 minutes which is enough to complete cell migration [29] in these examples. We assume a spherical shape for the cells with 24 finite element nodes on its membrane (Fig. 1-a). The properties of the cell and the substrate are listed in table 1. During migration, the centroid of each cell is visualized by a small sphere at each time step to indicate the cell position.

Table 1: Substrate and cell properties.

Description	Symbol	Value	Ref.
Poisson ratio	υ	0.3	[37, 17]
Viscosity	μ	1000 Pa.s	[37, 29]
Cell radius	r	20 μm	[38]
Stiffness of microtubules	K_{pas}	2.8 kPa	[39]
Stiffness of myosin II	K_{act}	2 kPa	[39]
Maximum strain of the cell	ε_{max}	0.09	[20, 31]
Minimum strain of the cell	ε_{min}	-0.09	[20, 31]
Maximum contractile stress exerted by actin-myosin machinery	σ_{max}	0.1 kPa	[40, 21]
Binding constant at the rear and front of the cell	$k_f = k_b$	10^8 mol^{-1}	[29]
Number of available receptors at the rear and front of the cell	$n_f = n_b$	10^5	[29]
Concentration of the ligands at rear and front of the cell	ψ	10^{-5}mol	[29]
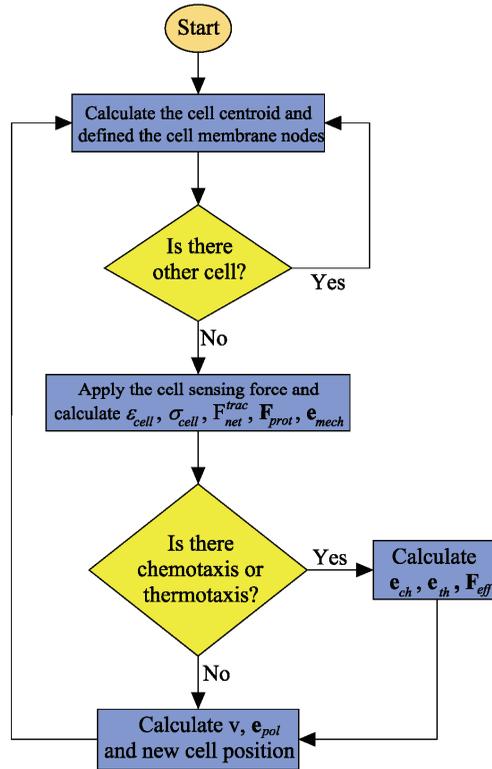
Figure 3: Computational algorithm of cell migration and cell-cell interaction considering mechanotaxis, chemotaxis, and/or thermotaxis.

3.1 Cell migration and cell-cell interaction in existence of pure mechanotaxis

Fig. 4 presents the migration trajectories of two cells under pure mechanotaxis in the above mentioned substrate. The cells are firstly located in different corners of the substrate where the substrate stiffness is minimum (80 kPa). As expected, the cells tendency is to migrate in the direction of the stiffness gradient towards higher stiffness. Because of the extended region between the two cells, they feel less internal deformation in this zone. Therefore, they firstly migrate towards each other to be in contact at $x = 85\ \mu$m. Once their polarization direction changes due to the protrusion force they get separated and migrate in the direction of the stiffness gradient. This phenomenon (contact and separation of the cells) can be repeated several times during their migration. Despite the maximum stiffness gradient of the substrate occurs at $x = 400\ \mu$m, the cells do not migrate towards the end of the substrate but they move around an imaginary equilibrium plane (IEP) orthogonal
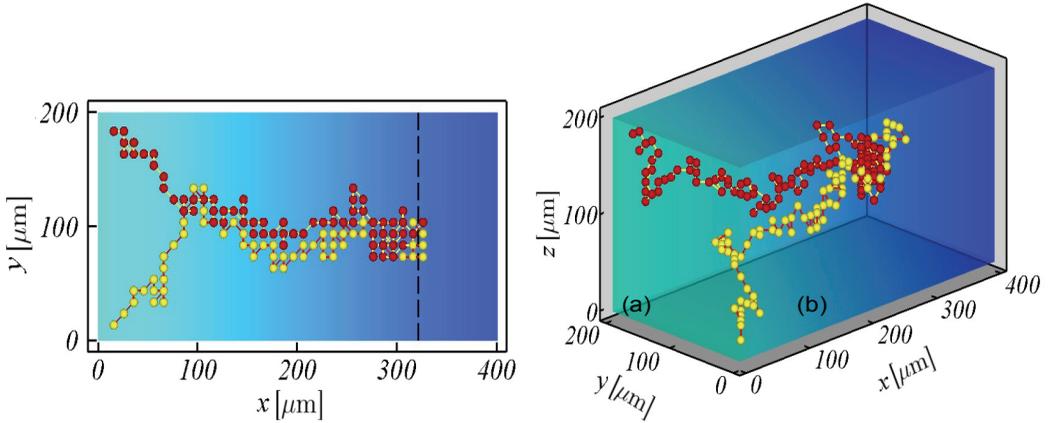
Figure 4: Cell migration and interaction due to pure mechanotaxis. A linear stiffness gradient has been considered from 80 kPa at $x=$ to 100 kPa at $x=$ 400 μm. Firstly the cells are located in different corners of the substrate near to $x=0$ where the substrate stiffness is minimal. The cells tendency is to contact each other and then they migrate towards higher stiffness. Finally the cells move around an IEP located far from the free surface at approximately $x=$ 325 μm.

to the stiffness gradient vector and located approximately at $x=$ 325 μm. The cells are able to recognize the free surface of the substrate as a soft and unstable region despite of the maximum stiffness of that zone [15, 16]. Any increase in the stiffness gradient slope will move the IEP towards the end of the substrate. In Figs. 5 and 6 the average net traction force and velocity of the cells are plotted versus average translocation of the cells. The results demonstrate that during cells migration towards more stable and stiffer regions, the average net traction force and the velocity of the cells reduce. This means that the cells tend to adhere to stiffer substrates and stay there almost with no locomotion [15, 20]. Reduction of the net traction force causes the cell to be a more spherical geometry [41], so cell stability increases in stiffer regions. It is remarkable that in very stiff substrates, the generated net traction forces may not be enough to move the cells to a new position. Besides, comparison of both curves with that of a single cell migration [20] demonstrates that the presence of two cells in a substrate with stiffness gradient increases the fluctuation of the curves since the contact and separation of the cells suddenly change the average traction force and velocity.

3.2   *Cell migration and cell-cell interaction with thermotaxis*

Higazi et al. [13] observed that trophoblast cells migrate towards warmer sites by means of thermotaxis in the absence of chemotaxis. Generally in vivo, thermotaxis is a complementary cue to chemotaxis [26]. Therefore this experiment is designed to investigate thermotactic effect son cell migration and cell-cell interaction (Fig. 7). It is assumed that there is a thermal gradient throughout the substrate in the *x* direction, which uniformly increases from 35°C at *x*=0, to 38°C at *x*=400 μm [13].
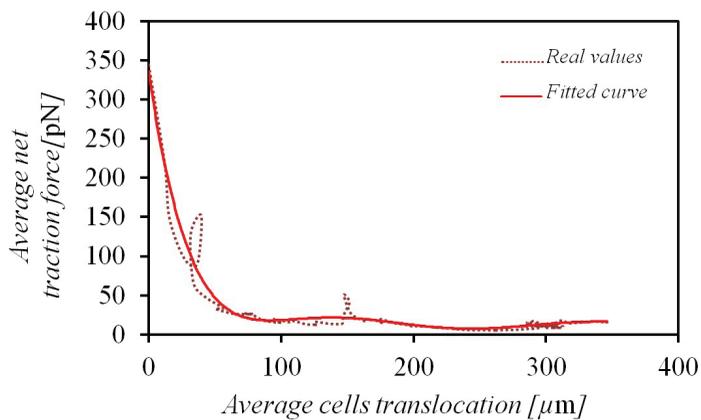
Figure 5: Average magnitude of the net traction force versus average translocation of the cells due to pure mechanotaxis.

We assumed μ_{th}=0.2. The results show that the existence of thermotaxis delays the contact between cells until *x*=115 μm (Fig. 7a). This is due to the fact that, besides the force pointing the cells towards each other (mechanotactic force) a part of the net traction force is directed by the thermotactic gradient that persistently guides the cells towards the warmer sites which inhibits relatively the cells to come in contact. In this case, as in the pure mechanotaxis case, contact and separation of the cells can repeat several times until they achieve warmer places. The migration of the cells towards warmer sites is consistent with findings of Higazi et al. [13]. It should be noted that due to the existence of the free boundary surface in the stiffer region of the substrate, again, the mechanotactic signal received by the cells dissuades them to move towards the warmest region of the substrate at *x*=400 μm. Consequently, thermotaxis causes the IEP to slightly move towards warmer site of the substrate so, in this case, it is located at *x*=335 μm approximately. Once the cells achieve this IEP they come in contact and separate repeatedly near the IEP.
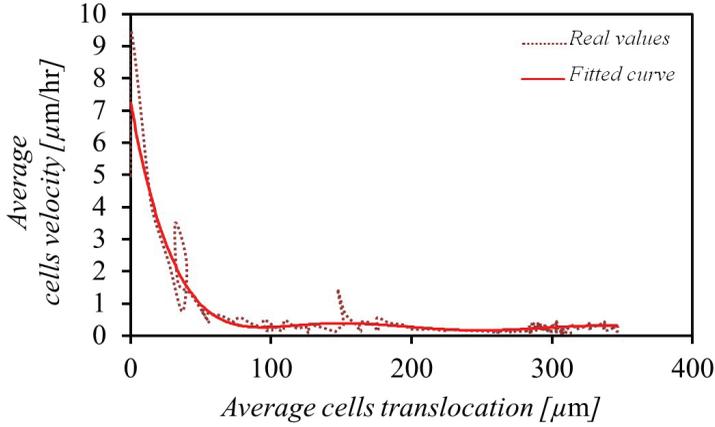
Figure 6: Average local velocity versus average translocation of the cells due to pure mechanotaxis.

Moreover, comparison of Figs. 7 with 4 indicates that the random movement of the cells through the substrate with thermotaxis gradient is relatively lower than that of pure mechanotactic migration.

Figs. 8 and 9 display the average magnitude of the net traction force and the local velocity of the cells versus the average translocation of the cells respectively As observed, during cell migration towards stiffer and warmer regions of the substrate both the magnitude of the net traction force and the cell local velocity decrease, having the same trend as in pure mechanotactic cell migration.

3.3 *Cell migration and cell-cell interaction with chemotaxis*

In this experiment, a chemotactic cue is added to the same substrate with stiffness gradient to assess the effect of a chemoattractant on cell migration and cell-cell interaction. It is assumed that there is a uniform chemical gradient along the x-axis increasing from zero at x=0 to 10^{-4}M at x= 400 μm. As before, the cells are located at different corners of the substrate near x=0 where the chemoattractan concentration is null. We assume that the chemotactic efficient factor is higher than the thermotactic one [9]. Fig. 10 presents the trajectory of the cells for $\mu_{ch} = 0.3$ and $\mu_{ch} = 0.4$. In this experiment the results indicate that existence of the chemoattractant cue in the substrate with gradient stiffness delays the cells contact even more than the thermotaxis due to the higher efficient factor. In this case, there exists an IEP too towards which the cells move. The location of this IEP is also sensitive to the chemotactic efficient factor. As observed in Fig. 10a, for μ_{ch}=0.3, the IEP dis-
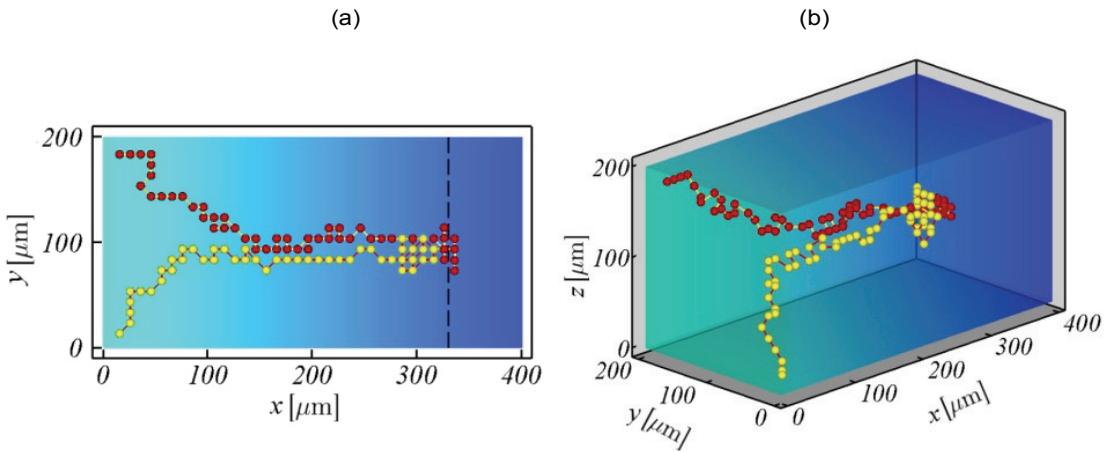
Figure 7: Cell migration and interaction in presence of thermotaxis. A linear thermal gradient along the *x* direction is assumed with maximum temperature (38°C) at *x*=400 μm . The thermal efficient factor is assumed to be 0.2. The cells are firstly placed in opposite corners of the substrate near *x*=0 with minimum temperature (35°C). They migrate towards warmer sites along the thermal gradient direction. Finally the cell keeps moving around an IEP located at *x*=335 μm approximately.
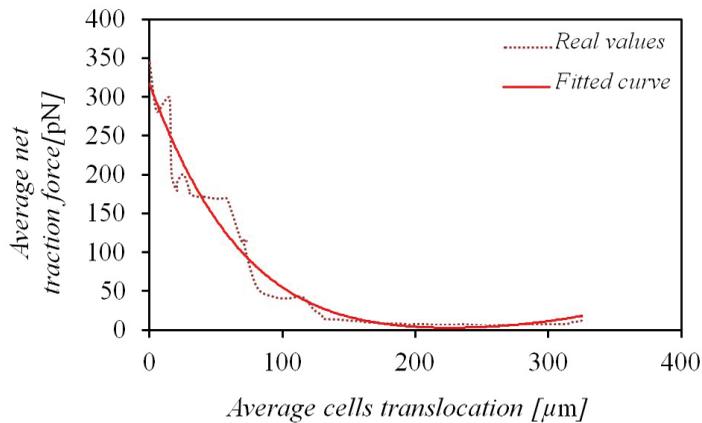
Figure 8: Average magnitude of the net traction force versus average translocation of the cells due to thermotaxis.
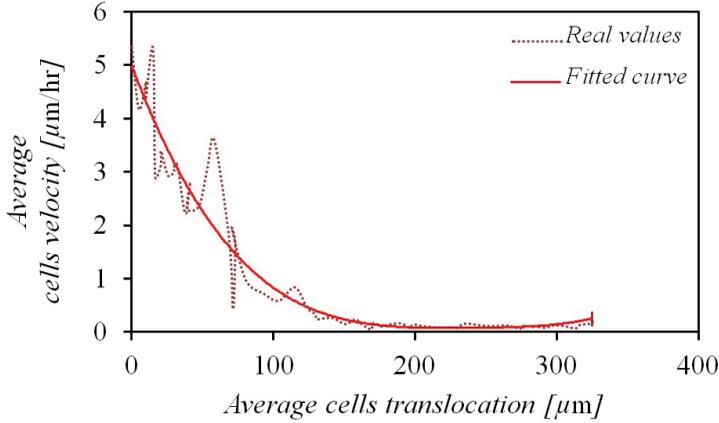
Figure 9: Average local velocity versus average translocation of the cells due to thermotaxis.

places towards the chemoattractant source (x= 355 μm) and becomes closer to the end of the substrate (x= 375 μm) when increasing the chemotactic efficient factor to 0.4 (Fig. 10c). It is remarkable that the closer the IEP becomes to the end of the substrate (higher efficient factor), the higher delay in cell contact. The existence of chemotaxis and mechanotaxis simultaneously also decreases the random movement of the cells throughout the substrate rather than in the cases of pure mechanotaxis or mechano-thermotaxis (compare Figs. 4 and 7 with 10). This occurs because of the received signals by the pseudopods of the cells strongly steer the cells in the chemotactic direction [22]. Consequently, as previously explained, the cell polarization direction which is persistently towards the chemoattractant source adds to the mechanotaxis effect thus increasing the cell global velocity. These results are in agreement with the experimental investigations of Andrew and Haaster [22, 42] who observed that in the presence of chemoattractant, depending on the signal strength of the chemotaxis, the cell can actively move towards chemoattractant sources. Moreover, similar cell behavior was reported by Bosgraaf et al. [9]. Our findings are also consistent with the numerical results of Neilson et al. [25].

Figs. 11 and 12 present the average net traction force and local velocity of the cells versus average translocation of the cells during chemotactic process. For both cases (μ_{ch}=0.3 and μ_{ch}=0.4), as in pure mechanotaxis migration, the cell net traction force and the cell local velocity decrease. This occurs because the magnitude of the net traction force is relatively independent of the chemotactic cue being function of the mechanical properties and boundary conditions of the substrate. On the other hand, the presence of chemotaxis (as thermotaxis) affects the drag force which

in turn can slightly reduce the cell velocity, although in this case, this reduction results negligible. Therefore, during cell migration towards stiffer regions and high chemoattractant concentration the behavior of the cells is similar to that of pure mechanotaxis in terms of average local velocity and magnitude of the net traction force.

3.4   *Cell migration and cell-cell interaction with chemotaxis and thermotaxis*

The last experiment is designed to consider the effect of all stimuli together on cell-cell interaction. It is assumed that there exist maximum chemoattractant concentration and temperature at x=400 μm which correspond to linear chemotactic and thermotactic gradients along the x axis. The cells are placed in opposite corners of the substrate near x=0. We assumed μ_{ch}=0.3 and μ_{th}=0.2. The results demonstrate that the existence of chemotaxis and thermotaxis together in the substrate (in addition to the gradient stiffness) delays the cells contact even more than in previous experiments (the cells first contact at x=265 μm as seen at 13a). The existence of chemotactic and thermotactic gradients in the same direction amplifies the signals received by the cells so that it drives them to migrate towards these cues, dominating cell-cell contact. As observed in Fig. 13, the IEP disappears and the cells migrate towards the free boundary at the end of the substrate. The presence of all stimuli together in the substrate causes the overall random movement of the cells to decrease even more than the previous experiments (compare Figs. 13 with 4, 7, 10). These results are in agreement with the chemotactic [42, 22] and thermotactic [26, 13] experimental investigations.

Figs. 14 and 15 present the average net traction force and local velocity of the cells versus average translocation of the cells during the mechano-chemo-thermotactic process. Similar to previous experiments, in the first time interval the average net traction force and local velocity of the cells decrease. This is due, as commented, to the relatively independent magnitude of the net traction force with respect to the chemotactic and thermotactic signals. On the contrary, the drag force, which is affected by all the combined mechanotactic, chemotactic and thermotactic efficient force, $\mathbf{F}_{eff}$ causes to very slightly reduce the cell velocity. In the last interval of these curves the average net traction force and local velocity of the cells increases due to the cells migration towards the free boundary surface (soft region).

4   Conclusions

Here, the previous computational model presented in [20] is extended to investigate the interaction of two cells migrating across a 3D substrate in the presence of mechanotactic, chemotactic and thermotactic cues. The model is based on the equilibrium of the different effective forces on cell motility. The generated traction

(a)

(b)

(c)

(d)
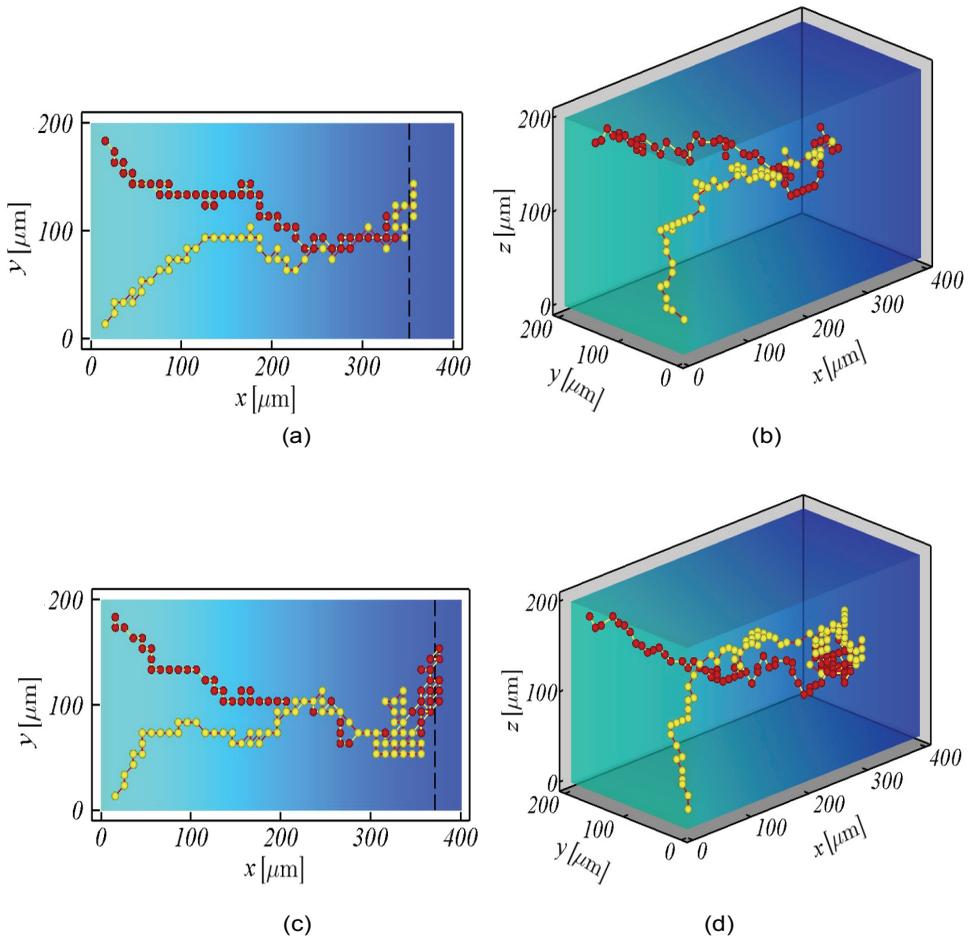
Figure 10: Migration and interaction of the cells with chemotaxis. It is assumed that a chemoattractant source at x=400 μm creates a linear chemoattractant gradient through the substrate along the $x$direction. Firstly the cells are located in different corners of the substrate near x=0 where the chemoattractant concentration is null. Cells migration is presented for two different chemoattractant efficient factors. In both cases, the cells migrate in the direction of the chemoattractant gradient towards an IEP When μ_{ch}=0.3 the IEP is located at x=355 μm approximately (a and b), while for μ_{ch}=0.4 the IEP displaces to x=375 μm approximately (c and d).
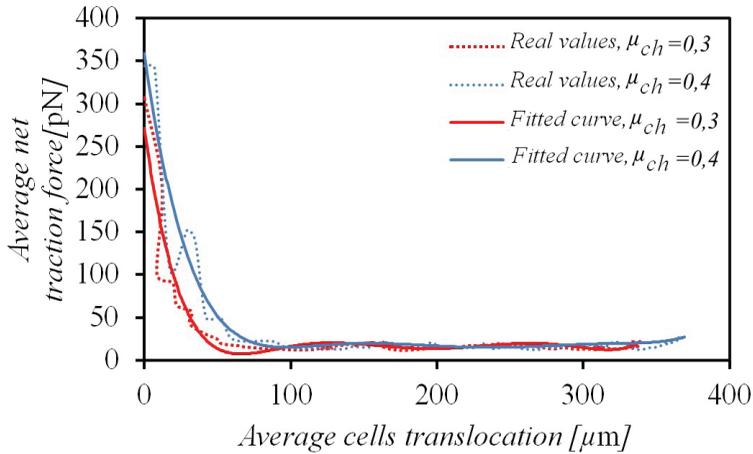
Figure 11: Average magnitude of the net traction force versus average translocation of the cells due to chemotaxis for $\mu_{ch} = 0.3$ and $\mu_{ch}=0.4$.
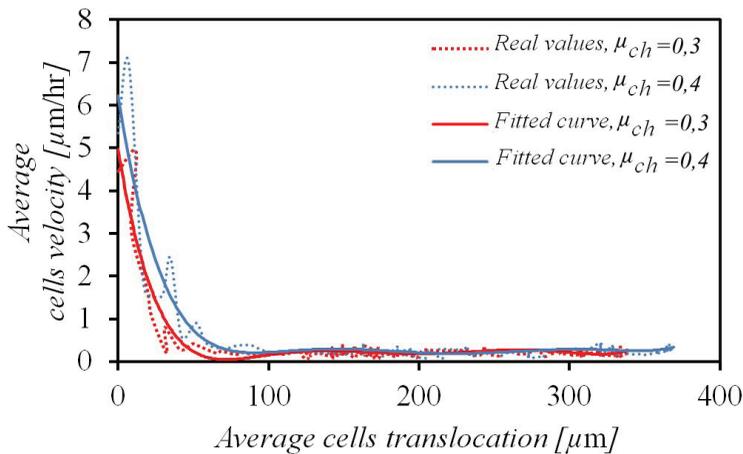
Figure 12: Average local velocity versus average translocation of the cells due to chemotaxis for $\mu_{ch} = 0.3$ and $\mu_{ch}=0.4$.

force during cell migration is derived from active signals inducing chemotaxis and thermotaxis in addition to initial mechanotaxis. We focused on the interaction of two cells during their migration through a substrate with linear stiffness gradient.

Under pure mechanotaxis, the cells tendency is first to reach each other and then migrate in the direction of the stiffness gradient towards an IEP [15, 16, 20, 43]. The IEP is located far from the free boundary surfaces, in a region that the cell mechanotransduction system "feels" more stable thus promoting a better cell adhesion [20]. The cells contact and separate several times during migration in the direction of the stiffness gradient, effect that will continue in the final residence region close to the IEP.

(a)   (b)
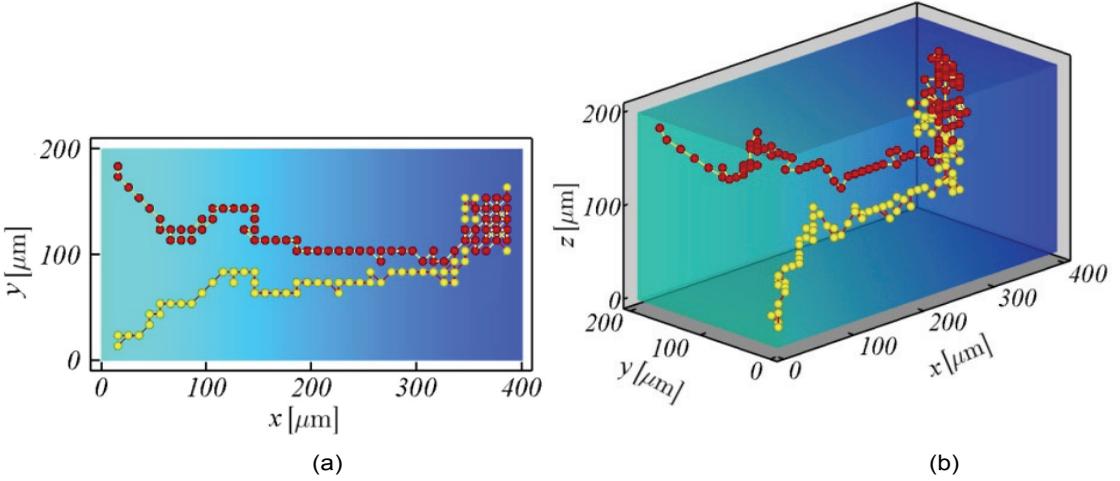
Figure 13: Migration and interaction of the cells with chemotaxis and thermotaxis. It is assumed that the chemoattractant concentration and temperature at x=400 μm are maximal. Two linear chemotactic and thermotactic gradients are assumed through the substrate along the x direction. Firstly the cells are located in the different corners of the substrate near x=0 where the chemoattractant concentration is null and the temperature is minimal. μ_{ch}=0.3 and μ_{th}=0.2. In this case the IEP disappears and the cells migrate towards the maximum chemoattractant concentration and temperature.

The study of the chemotactic and/or thermotactic effects on cell migration demonstrate that the IEP location is sensitive to the corresponding efficient factors. Under thermotaxis, the IEP slightly displaces towards warmer sites, while adding chemotaxis further displace the IEP to the end of the substrate. Besides, IEP can even
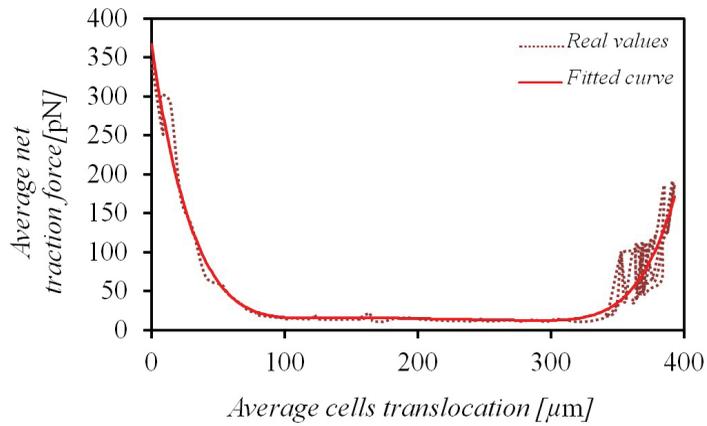
Figure 14: Average magnitude of the net traction force versus average translocation of the cells due to chemotaxis and thermotaxis. μ_{ch}=0.3 and μ_{th}=0.2.
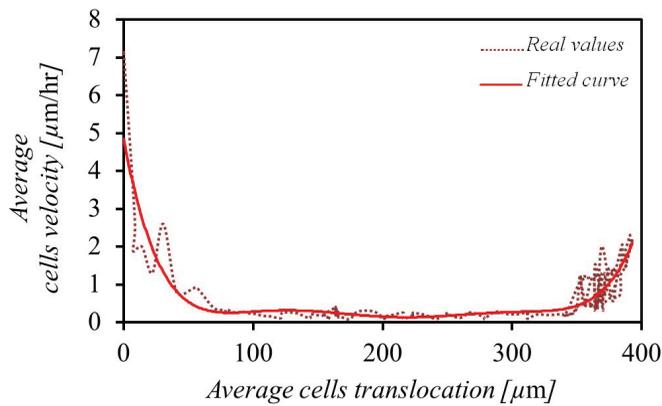
Figure 15: Average local velocity versus average translocation of the cells due to chemotaxis and thermotaxis. μ_{ch}=0.3 and μ_{th}=0.2.

vanish with higher or reinforcing signals as in the case here analyzed with combined reinforcing mechanotatic, chemotactic and thermotactic cues. This reinforcing joint chemotaxis and thermotaxis may dominate the mechanotactic signal thus propelling the cell towards the chemoattractant source with maximum temperature. It is remarkable that the effect of these cues on the cell local velocity is negligible. This is because the magnitude of the net traction force is function only of the surrounding mechanical conditions and substrate properties. In addition, the presence of chemotactic and/or thermotactic signals delays contact of the cells because these cues persistently steer the cells towards high chemoattractant concentration and/or warmer sites. Therefore, the higher efficient factors of cues, the less contact between cells. These findings are in agreement and consistent with the chemotaxis experiments presented in [9, 22, 42] and thermotaxis [13, 26].

The results obtained and discussed herein are also qualitatively consistent with the experimental works [9, 13, 15, 16].

To conclude, the present model enables to predict a wide range of experimental observations. It is highly flexible in terms of cell shape, number of cells and multisignal analysis of cell migration. The obtained results depend much on the choice of the parameters such as chemotactic and thermotactic efficient factors which can be calibrated with further experimental works. Moreover, the present mechano-chemo-thermotactic model can be used to examine a wider range of efficient signals affecting cell migration such as durotaxis, haptotaxis and topotaxis. As main limitation is the poor knowledge of some of the parameters involved and the scarcity of experimental data in different conditions that could serve to quantitatively validate or refuse some of the conclusions here summarized.

References

1. H. Behesti and S. Marino. Cerebellar granule cells: Insights into proliferation, differentiation, and role in medulloblastoma pathogenesis. *Journal Applied Physiology* 41:435–445, 2009.

2. B.A. Dalton, X.F. Walboomers, M. Dziegielewski, M.D.M. Evans, S. Taylor, J.A. Jansen, and J.G. Steele. Modulation of epithelial tissue and cell migra-

tion by microgrooves. *Phil. Trans. Roy. Soc. London* 56:195–207, 2001.

3. T. Pompe, S. Glorius, T. Bischoff, I. Uhlmann, M. Kaufmann, S. Brenner, and C. Werner. Dissecting the impact of matrix anchorage and elasticity in cell adhesion. *Biophysical Journal*, 97:2154–2163, 2009.

4. S. Suresh. Biomechanics and biophysics of cancer cells. *Acta Biomaterialia* 3:413–438, 2007.

5. M. Zhao. Electrical fields in wound healing-an overriding signal that directs cell migration. *Seminars in Cell and Developmental Biology* 20:674–82, 2009.

6. R. Allena and D. Aubry "run-and-tumble" or "look-and-run"? a mechanical model to explore the behavior of a migrating amoeboid cell. *Journal of Theoretical Biology* 306:15–31, 2012.

7. B.K. Chirag, R.P Shelly and J.P Andrew. Intrinsic mechanical properties of the extracellular matrix affect the behavior of pre-osteoblastic mc3t3-e1 cells. *Am J Physiol Cell Physiol* 290:C1640–C1650, 2006.

8. R.J. Pelham, Jr., and Y.L. Wang. Cell locomotion and focal adhesions are regulated by substrate flexibility *PNAS* 94:13661–13665, 1997.

9. L. Bosgraaf and P.J.M. Van Haastert. Navigation of chemotactic cells by parallel signaling to pseudopod persistence and orientation. *PLoS ONE* 4:e6842, 2009.

10. O. Hoeller and R.R. Kay Chemotaxis in the absence of pip3 gradients. *Current Biology* 17:813–817, 2007.

11. M.P Neilson, D.M. Veltman1, P.J.M. van Haastert, S.D. Webb, J.A. Mackenzie, and R.H. Insall. Chemotaxis: A feedback-based computational model robustly predicts multiple aspects of real cell behaviour. *PLoS Biol* 9:e1000618, 2011.

12. B.H. Choo, R.F. Donna, and L.P Kenneth. Thermotaxis of dictyostelium discoideum amoebae and its possible role in pseudoplasmodial thermotaxis. *Proc. Natl. Acad. Sci. USA* 80:5646–5649, 1983.

13. A.A. Higazi, D. Kniss, J. Manuppelloand E.S. Barnathan, and D.B.Cines. Thermotaxis of human trophoblastic cells. *Placenta* 17:683–7, 1996.

14. Y.T. Maeda, J. Inose, M.Y. Matsuo, S. Iwaya, and M. Sano. Ordered patterns of cell shape and orientational correlation during spontaneous cell migration. *PLoS ONE* 3:e3734, 2008.

15. E. Hadjipanayi, V. Mudera, and R.A. Brown. Guiding cell migration in 3d: A collagen matrix with graded directional stiffness. *Cell Motility and the Cytoskeleton* 66:435–445, 2009.

16. C.M. Lo H.B. Wang, M. Dembo, and Y.L. Wang. Cell movement is guided by the rigidity of the substrate. *Biophysical Journal* 79:144–152, 2000.

17. T.A. Ulrich, E.M. De Juan Pardo, and S. Kumar. The mechanical rigidity of the extracellular matrix regulates the structure, motility and proliferation of glioma cells. *Cancer Research* 69:4167–4174, 2009.

18. D.E. Ingber and I. Tensegrity Cell structure and hierarchical systems biology *Journal Cell Science* 116:1157–1173, 2003.

19. P Moreo, J.M. Garcia-Aznar, and M. Doblaré. Modeling mechanosensing and its effect on the migration and proliferation of adherent cells. *Acta Biomaterialia* 4:613–621, 2008.

20. S.J. Mousavi, M.H. Doweidar, and M. Doblaré. Computational modelling and analysis of mechanical conditions on cell locomotion and cell-cell interaction. *Comput Methods Biomech Biomed Engin.* page DOI: 10.1080/102558422012.710841, 2012.

21. C.G. Penelope and P.A. Janmey Cell type-specific response to growth on soft materials. *Journal Applied Physiology* 98:1547–1553, 2005.

22. P.J.M. Van Haastert. Chemotaxis: insights from the extending pseudopod. *J Cell Sci.* 123:3031–37, 2010.

23. K.F. Swaney C.H. Huang, and P.N. Devreotes. Eukaryotic chemotaxis: a network of signaling pathways controls motility directional sensing, and polarity *Annu Rev Biophys* 39:265–289, 2010.

24. S. Zhang, P.G. Charest, and R.A. Firtel. Spatiotemporal regulation of ras activity provides directional sensing. *Curr. Biol* 18:1587–93, 2008.

25. M.P Neilson, J.A. Mackenzie, S.D. Webb, and R.H. Insall. Modeling cell movement and chemotaxis using pseudopod-based feedback. *SIAM Journal on Scientific Computing* 33:1035–1057, 2011.

26. M. Eisenbach A. Bahat. Sperm thermotaxis. *Molecular and Cellular Endocrinology* 252:115–119, 2006.

27. G.B. Young. Thermography *CRC Critical Reviews of Radiological Science* 1:593–638, 1970.

28. C.B. Hong, D.R. Fontanat, and K.L. Pofft. Thermotaxis of dictyostelium discoideum amoebae and its possible role in pseudoplasmodial thermotaxis. *Proc. Natl. Acad. Sci* 80:5646–49, 1983.

29. M.H. Zaman, R.D. Kamm, P Matsudaira, and D.A. Lauffenburgery Computational model for cell migration in three-dimensional matrices. *Biophysical Journal* 89:1389–1397, 2005.

30. D.W. James and J.F. Taylor. The stress developed by sheets of chick fibroblasts in vitro. *Experimental Cell Research* 54:107–110, 1969.

31. S. Ramtani. Mechanical modelling of cell/ecm and cell/cell interactions during the contraction of a fibroblast-populated collagen microsphere:theory and model simulation. *Journal of Biomechanics* 37:1709–1718, 2004.

32. R.C. Gao, X.D. Zhang, Y.H. Sun, Y. Kamimura, A. Mogilner, P.N. Devreotes, and M. Zhao. Different roles of membrane potentials in electrotaxis and chemotaxis of dictyostelium cells. *Eukaryotic Cell* 10:doi: 10.1128/EC.05066–11, 2011.

33. E. Palsson. A three-dimensional model of cell movement in multicellular systems. *Future Generation Computer System* 17:835–852, 2001.

34. G.W. Brofland and C.J. Wiebe. Mechanical effects of cell anisotropy on epithelia. *Computer Methods Biomech. Biomed. Engin.* 7:91–99, 2004.

35. D.L. Taylor, J. Heiple, Y.L. Wang, E.J. Luna, L. Tanasugarn, J. Brier, J. Swanson, M. Fechheimer, P Amato, M. Rockwel, and G. Daley Cellular and molecular aspects of amoeboid movement. *CSH Symp. Quant. Biol.* 46:101–111, 1982.

36. Hibbit, Karlson, and Sorensen. *Abaqus-Theory manual* 6.3 edition edition.

37. S.K. Akiyama and K.M. Yamada. The interaction of plasma fibronectin with fibroblastic cells in suspension. *Journal of Biological Chemistry* 260:4492–4500, 1985.

38. A. Buxboim, I.L. Ivanovska, and D.E. Discher. Matrix elasticity cytoskeletal forces and physics of the nucleus: how deeply do cells 'feel' outside and in? *Journal of cell science* 123:297–308, 2010.

39. A. Schäfer and M. Radmacher. Influence of myosin ii activity on stiffness of fibroblast cells. *Acta Biomaterialia* 1:273–280, 2005.

40. G.F. Oster, J.D. Murray and A.K. Harris. Mechanical aspects of mesenchymal morphogenesis. *journal Embryol Exp Morph* 78:83–125, 1983.

41. M. Ehrbar, A. sala, P Lienemann, A. Ranga, K. Mosiewicz, A. Bittermann, S. C. Rizzi, and F. E. Weber. Elucidating the role of matrix stiffness in 3d ceell migration and remodeling. *Biophysical Journal* 100:284–293, 2011.

42. N. Andrew and R.H. Insall. Chemotaxis in shallow gradients is mediated independently of ptdlns 3-kinase by biased choices between random protrusions. *Nature Cell Biology* 9:193–200, 2007.

43. D.K. Schlüter, I.R.C., and M.A.J. Chaplain. Computational modeling of single-cell migration: The leading role of extracellular matrix fibers. *Biophysical Journal* 103:1141–51, 2012.